Cardiac motion estimation using multi-scale feature points

Release 0.00

Alessandro Becciu, Hans C. van Assen, Luc Florack, Bart J. Janssen and Bart M. ter Haar Romeny

May 21, 2008

Eindhoven University of Technology, Eindhoven, The Netherlands

Abstract

Heart illnesses influence the functioning of the cardiac muscle and are the major causes of death in the world. Optic flow methods are essential tools to assess and quantify the contraction of the cardiac walls, but are hampered by the aperture problem. Harmonic phase (HARP) techniques measure the phase in magnetic resonance (MR) tagged images. Due to the regular geometry, patterns generated by a combination of HARPs and sine HARPs represent a suitable framework to extract landmark features. In this paper we introduce a new aperture-problem free method to study the cardiac motion by tracking multi-scale features such as maxima, minima, saddles and corners, on HARP and sine HARP tagged images.

Contents

1 Introduction

Cardiovascular diseases may seriously influence the heart function, altering its regular wall deformation and increasing the risk of heart failure. In 2004 heart diseases were responsible of more than 850.000 deaths only in the US; they formed the major cause of death for the US population and generated healthcare costs of hundreds of billions of dollars [19]. In this context, there is a necessity to assess the detailed motion of cardiac tissue, using this as an indicator for the progress of disease and/or for the response to therapy and perhaps even as precursors of cardiac symptoms. Optic flow is one of the traditional techniques in carrying out motion analysis. Optic flow measures the apparent velocity pattern of moving structures in an image sequence. In computer vision literature, several optic flow approaches have been described, ranging from gradient based techniques to feature based methods. Differential techniques compute the velocity from spatiotemporal image intensity derivatives or filtered versions of the image, using low-pass or band-pass filters. In most of these techniques it is assumed that brightness does not change by small displacements and the motion is estimated by solving the so-called Optic Flow Constraint Equation (OFCE):

$$L_x u + L_y v + L_t = 0 \tag{1}$$

where $L(x,y,t) : \mathbb{R}^3 \rightarrow \mathbb{R}$ is an image sequence, L_x, L_y, L_t are the spatiotemporal derivatives, $u(x,y,t), v(x,y,t) : \mathbb{R}^3 \rightarrow \mathbb{R}$ are unknown velocity vectors and x, y and t are the spatial and temporal coordinates respectively. Since there is one equation and two unknowns (u and v), a unique solution cannot be found. This has been referred as the "aperture problem". In order to find a plausible solution for equation (1), Horn and Schunck [12] combined the gradient constraint with a global smoothness term, finding the solution by minimizing an energy function. Lucas and Kanade [15] proposed a local differential technique, for which the flow field is constant in a small spatial neighborhood. The results obtained by the early methods were impressively improved by Brox et al. and Bruhn et al. [5, 6], who investigated a continuous, rotationally invariant energy functional and giving a multi-grid approach to the variational optical flow methods. Florack et al. [9, 8] developed a robust differential technique in a multi-scale framework. An application of this technique to cardiac MR images was presented by Niessen et al [17, 16] and Suinesiaputra et al. [22]. Van Assen et al. and Florack et al. [1, 11] developed a method based on multiple independent MR tagging acquisitions, removing altogether the aperture problem, by generating as many equations as unknowns.

Standard OFCE methods are underconstrained, and need additional assumptions. In this paper we investigate cardiac motion by exploiting point features in Gaussian scale-space. These features are interesting candidates for motion analysis: for those points the aperture problem does not arise and they are detected in a robust framework, which is inspired by findings of the multi-scale structure of the visual system. In the experiments maxima, minima, saddles and corners are chosen as feature points and the approach has been tested on an artificial and real sequence. Outcomes of the proposed technique emphasize the reliability of the vector field.

In sections 2 and subsection 2.1 a preprocessing approach and the multi-scale framework used in the experiments is presented. In 2.2 the topological number will be introduced as a convenient technique for extracting multi-scale features. In 2.3, 2.4 and 2.5, we present the corner detection method, the calculation of a sparse velocity vector field, the dense flow field extension and the angular error measure. Finally in section 3 and 4 we describe the experiment, the results and discuss the future directions.

2 Method

The experiments were carried out on a sequence of tagged MR images of a mouse heart's left ventricle. In 1988 Zerhouni et al. [24] introduced a tagging method for noninvasive assessment of myocardial motion. The method introduces structure, represented as dark stripes (figure 1 top), on the image aiming to improve the visualization of the intramyocardial motion. The approach was later improved by Axel et al. and Fischer et al [2, 7], who explored magnetic resonance imaging using spatial modulation of magnetization (SPAMM) and (CSPAMM) respectively. The images, however, suffer from tag fading, making the frames not suitable for optic flow methods based on conservation of brightness. In the harmonic phase (HARP) method [18, 20], MR images are filtered in the spectral domain and this technique overcomes the fading problem by taking into account the spatial phase information from the inverse transform of the filtered images. In our experiments the HARP technique was employed. Two tagged image series with mutually perpendicular tag lines were acquired (Figure 1 Top) and the first harmonic peak was filtered out using a band-pass filter in the Fourier domain (Figure 1 middle). Once applied the inverse Fourier transform, in the filtered images the phase varies periodically from 0 to 2π creating a saw tooth pattern (Figure 1 fourth from the top, left and middle picture). The combination of frames with horizontal and vertical stripes was used to create a grid pattern, which allowed the extraction of corners (Figure 1 fourth from the top, right picture). A sine function was applied to the phase images so as to avoid spatial discontinuities in the input due to the saw tooth pattern. A combination of sine HARP frames was later employed to produce a grid, from which the features points (maxima, minima and saddles) were retrieved (Figure 1 Bottom).

2.1 Scale Space

Scale is one of the most important concepts in human vision. When we look at a scene, we instantaneously view its contents at multiple scale levels. The Gaussian scale-space representation $L(x,y,s) \in \mathbb{R}^2 \times \mathbb{R}^+$ of a raw 2-dimensional image $f(x,y) \in \mathbb{R}^2$ is defined by the convolution of $f(x,y)$ with a Gaussian kernel $\phi(x,y,s) \in \mathbb{R}^2 \times \mathbb{R}^+$.

$$L(x,y,s) = (f * \phi)(x,y,s) \tag{2}$$

where $\phi(x,y,s) = \frac{1}{4\pi s}\exp(-\frac{x^2+y^2}{4s})$. In equation (2) x and y are the spatial coordinates, whereas $s \in \mathbb{R}^+$ denotes the variance of the Gaussian kernel (scale). Equation (2) provides a blurred version of the image, where the strength of blurring depends on the choice of scale. For an extensive review on scale space see [8, 13, 23, 14].

2.2 Topological Number

Singularities (critical points) induced by the MR tagging pattern are interesting candidates for structural descriptions. Detection and classification of critical points can be performed in an efficient way by the computation of the so-called topological number [23, 21].

We examine a point P in image L and its neighborhood N_P. Suppose that N_P does not have any other critical points with exception of the point P itself, and suppose ∂N_P is the boundary of N_P, which is a D-1 dimensional oriented closed hypersurface. Since there are no critical points at ∂N_P, the normalized gradient of the image L on ∂N_P is defined component-wise as: $\xi_i = \frac{L_i}{\sqrt{L_j L_j}}$ with $L_i = \partial_i L$ and $i = 1,...,D$ (summation convention applies. Here we have $D = 2$). For a non-singular point we may define the D-1 dimensional form

$$\Phi = \xi_{i_1} d\xi_{i_2} \wedge ... \wedge d\xi_{i_D} \varepsilon^{i_1 ... i_D} \tag{3}$$

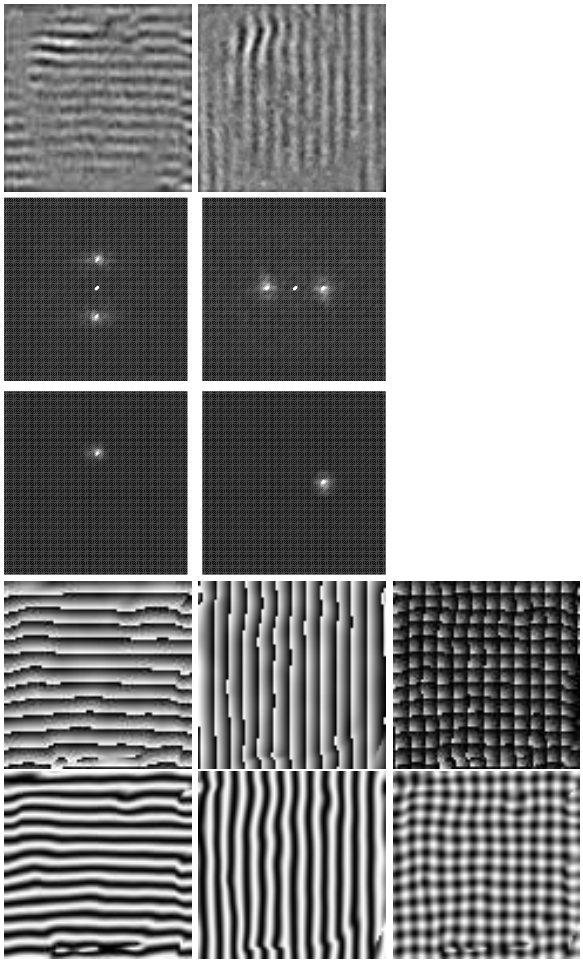

Figure 1: Top: cardiac mouse MR tagged images with horizontal and vertical tags. Second from the top: Fourier transform of cardiac mouse MR tagged images with horizontal and vertical tags. Middle: filtered harmonic peak by using a band-pass filter. Fourth from the top: harmonic phase (HARP), the phase varies periodically from 0 to 2π creating a saw tooth pattern. Grid obtained by combining the vertical with the horizontal tags of the HARP images. Bottom: sine HARP images and grid obtained by combining the vertical with the horizontal stripes.

where the symbol "$\wedge$" represents the wedge product and $\varepsilon^{i_1\ldots i_D}$ is the permutation tensor of order D such that: $\varepsilon^{i_1\ldots i_l\ldots i_k\ldots i_D} = -\varepsilon^{i_1\ldots i_l\ldots i_k\ldots i_D}$ $\forall$l$\neq$k and $\varepsilon^{12\ldots D} = 1$. Making the substitution of ξ_i in Φ we obtain:

$$\Phi = \frac{L_{i_1} dL_{i_2} \wedge \ldots \wedge dL_{i_D} \varepsilon^{i_1\ldots i_D}}{(L_j L_j)^{D/2}} \tag{4}$$

The topological number can then be defined as

$$\nu_{\partial N_P} = \frac{1}{A_D} \oint_{x\varepsilon\partial N_P} \Phi(x) \tag{5}$$

where A_D represents the area enclosed by ∂N_P.

In two-dimensional images the topological point is referred as the *winding number* and represents the integrated change of angle of the gradient when traversing a closed curve in a plane. In two dimensions,

equation (3) and (5) can be represented in a convenient way using the complex numbers. Given the complex couple of coordinates $z = x + \mathrm{i}y$ and the complex conjugate $\bar{z} = x - \mathrm{i}y$, the gradient vector field of the image $L(z,\bar{z})$ can be expressed as $W = (L_x + \mathrm{i}L_y)/2 \equiv \partial_{\bar{z}} L(z,\bar{z})$. Hence, expression (3) can be written as

$$\Phi = \xi_x d\xi_y - \xi_y d\xi_x = \frac{L_x dL_y - L_x dL_y}{L_x L_x + L_y L_y} = \mathrm{Im}\frac{(L_x - \mathrm{i}L_y)d(L_x + \mathrm{i}L_y)}{L_x L_x + L_y L_y} = \mathrm{Im}(\frac{dW}{W}) = \mathrm{Im}(d\ln W) \tag{6}$$

where $\ln W = \ln \mid W \mid + \mathrm{i}\arg W$. Φ can, therefore, be read as the angle change of the gradient field.

The winding number is always an integer times 2π and classifies singularities of a scalar image at any dimension. For regular points the winding number is zero, for extrema the winding number is $+2\pi$, whereas for saddle points is -2π. Figure 2 shows gradient vector fields and winding number path for maxima, minima, saddle, and regular points respectively.

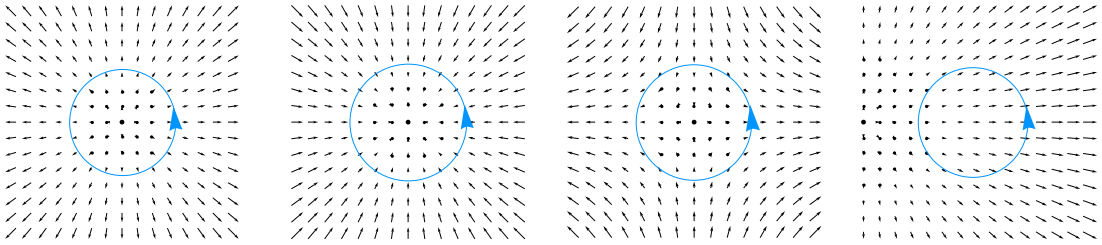

Figure 2: Gradient vector fields and winding number path for maxima, minima, saddle, and regular points respectively.

Algorithm 1 Winding number

1: Define the complex gradient as $L_x + \mathrm{i}L_y$, where the derivatives are taken in scale-space.
2: For every pixel, extract the complex gradient with respect to the 8 neighbor pixels.
3: Extract the winding number
4: Check the sign of the winding number. Consider only winding numbers greater or smaller than 0.
5: If the sign of the winding number is positive, there is an extrema, else a saddle point.
6: In case of extrema, check the sign of the second order derivatives of the image at those points. In case the sign is negative, there is a maximum, else a minimum.

2.3 Corner Detection

From differential geometry, image descriptors can easily be represented by a coordinate system, known as gauge coordinate system, which is dependent on the local structure of the image. One component $\vec{\mathrm{v}} = \{\frac{\partial L}{\partial x}, \frac{\partial L}{\partial y}\}$ is everywhere perpendicular to the isophote (line with constant intensity) and points in the direction of the gradient vector, the other component $\vec{\mu}$ is tangential to the isophote such that $\vec{\mu} = \{\frac{\partial L}{\partial y}, -\frac{\partial L}{\partial x}\}$.

In computer vision a corner is defined as a point with high isophote curvature and high intensity gradient. The curvature gives a measure of local deviation from the tangent line and in gauge coordinates is described as: $k = -\frac{L_{\mu\mu}}{L_{\mathrm{v}}}$. Hence, a corner detector is defined as: $\Theta^n = -\frac{L_{\mu\mu}}{L_{\mathrm{v}}} L_{\mathrm{v}}^n$. In case of $n = 3$, Θ provides the so-called (volume preserving) affine invariant corner detector [23, 4, 10].

$$\Theta^3 = -\frac{L_{\mu\mu}}{L_{\mathrm{v}}} L_{\mathrm{v}}^3 = -2L_x L_{xy} L_y + L_{xx} L_y^2 + L_x^2 L_{yy} \tag{7}$$

In the experiments the maxima of the corner response were used as feature points.

2.4 Sparse Velocities of Feature Points and Dense Flow Field

In our experiments given a sequence of frames, we assume that the singularity (feature) points move along with the moving tissue (this is true by construction of the tagging pattern, provided the feature points correctly correspond to the tag crossings and to the corners of the tag crossings). In general, given a point in a sequence of frames defined as $L(x(t),y(t),t)$, where t indicates the time, the critical points are defined implicitly by a vanishing spatial gradient:

$$\nabla L(x(t),y(t),t) = 0 \tag{8}$$

In order to track the feature points, we derive equation (8) with respect to time and apply the chain rule for implicit functions, yielding:

$$\frac{d}{dt}\left[\nabla L(x(t),y(t),t)\right] = \begin{bmatrix} L_{xx}u + L_{xy}v + L_{xt} \\ L_{xy}u + L_{yy}v + L_{yt} \end{bmatrix} = 0 \tag{9}$$

where $\frac{d}{dt}$ is the total time derivative, and where we have dropped space-time arguments on the r.h.s. for simplicity. Equation (9) holds only on location of critical points and can be also written as:

$$\begin{bmatrix} u \\ v \end{bmatrix} = -H^{-1}\frac{d\nabla L}{dt} \tag{10}$$

where H denotes the Hessian matrix of $L(x(t),y(t),t)$.

The velocities computed by equation (10) represent the flow field at a sparse set of positions. In order to retrieve a dense velocity field, the sparse velocities have been interpolated using homogeneous diffusion interpolation. Given a spatial domain $\Omega \rightarrow \mathbb{R}^2$, the scalar functions $u(x,y)$ and $v(x,y)$ are the horizontal and vertical components of a velocity vector $V : \Omega \rightarrow \mathbb{R}^2$. We know the velocity vectors just at certain positions and we call these vectors $\tilde{V} = \{\tilde{u},\tilde{v}\}$ such that $\tilde{V} : \Omega_s \rightarrow \mathbb{R}^2$, where Ω_s is a finite subset of Ω. We are interested in retrieving a dense set of vectors $V\ \forall x,y \in \Omega$. In order to do so, we minimize the energy function

$$E(u,v) = \int_\Omega (\parallel \nabla u(x,y) \parallel^2 + \parallel \nabla v(x,y) \parallel^2) dxdy \tag{11}$$

under the constraint $V = \tilde{V}\ \forall x,y \in \Omega_s$. The minimization of equation (11) is carried out by employing Euler-Lagrange equations and the resulting expression can be solved with numerical schemes.

Algorithm 2 Computation velocities

1: Calculate set of velocities by solving (10) only for maxima, minima, saddle points and corners.
2: Determine the velocity of other points by minimizing (11).
3: Interpolate separately the x and the y components of the velocity vectors.

2.5 Angular Error

The interpolated flow vector at certain positions in the image can deviate from the true flow vector at that position in direction and in length. In our assessment we are interested in the movement from one frame to the next. Therefore, we set the time component of the flow vector to 1, yielding a 3-dimensional vector $V = \{u,v,1\}$. The computed vector field has been compared with a ground truth extracted by an artificial

sequence described in section 3 and the assessment has been performed using the so-called average angular error (AAE) introduced by Barron et al. [3]

$$\text{Angular Error} = \arccos\left(\frac{V_t}{\sqrt{u_t^2+v_t^2+1}} \cdot \frac{V_e}{\sqrt{u_e^2+v_e^2+1}}\right) \tag{12}$$

where V_t is the true vector with spatial component u_t, v_t and time component 1, whereas V_e is the estimated velocity vector and u_e, v_e and 1 are its spatial and time components respectively.

3 Results

The proposed optic flow method was applied on a real sequence of 7 MR images (Figure 2), representing a mouse heart in phase of contraction. The images presented a resolution of 80 by 80 pixels and contained tags of 8 pixels wide; this width has been used to choose a physically reasonable range of spatial scales at which the features and the velocity field were calculated. The spatial scale is defined as $\sigma = \sqrt{2s}$ and the experiments were performed from spatial scale $\sigma = 1$ until scale $\sigma = 8$ at time scale 1. In order to asses the extracted vector field, an artificial sequence of 11 frames obtained by combination of translations (with rate of 1 pixel per frame) in different directions was created, using the first frame of HARP and Sine HARP and grid images (Figure 1, Fourth from the top (right) and Bottom (right)). A comparison between the extracted vector field and the ground truth is shown in figure 3. In Table 1 are displayed the performance of the proposed method, by the employment of different multi-scale features. In order to avoid outliers due to boundary conditions, the computation of the flow field was performed from frame 5 to frame 8 and the assessment was carried out on flow field regions 10 pixels distant from the boundaries. Finally, the error has been expressed in terms of "Average Angular Error" (AAE) and its standard deviation. The proposed method achieved the best performance by employing all the feature points (AAE $= 2 \times 10^{-2}$degrees and Std $= 3 \times 10^{-2}$degrees).

Feature	M1	M2	S	C	M1 M2	M1 S	M1 C	M2 S	M2 C	S C	M1 M2 S	M1 M2 C	M1 S C	M2 S C	M1 M2 S C
AAE	1.31°	1.44°	0.28°	1.27°	0.26°	0.09°	0.25°	0.1°	0.58°	0.09°	0.03°	0.12°	0.03°	0.05°	0.02°
Std	0.90°	1.02°	0.31°	0.93°	0.27°	0.13°	0.26°	0.13°	0.55°	0.12°	0.04°	0.05°	0.04°	0.07°	0.03°

Table 1: Performance of the proposed optic flow method with different multi-scale feature points. M1:Maxima, M2:Minima, S: Saddle, C: Corners. In the experiments the Average Angular Error (AAE) and its standard deviation have been employed as error measurement. The error measure is expressed in degrees. The scales used in the experiment were: spatial scale $\sigma = \{1, 1.25992, 1.5874, 2., 2.51984, 3.1748, 4., 5.03968, 6.3496, 8.\}$, time scale 1

4 Discussion

In this paper we propose a new method to track cardiac motion from a combination of HARP and Sine HARP images by following the movement of multi-scale singularity points. Qualitative and quantitative analysis of the results emphasize the reliability of the vector field, in particular, we found that the accuracy of the flow field is dependent on the number of the employed features. The best performance has been achieved by using all features simultaneously AAE $= 2 \times 10^{-2}$degrees. For a more reliable results, however, in the forthcoming experiments we will assess the approach by using more complex test image sequences and compare it with constant brightness based methods. Furthermore, it is interesting to point out, that constant

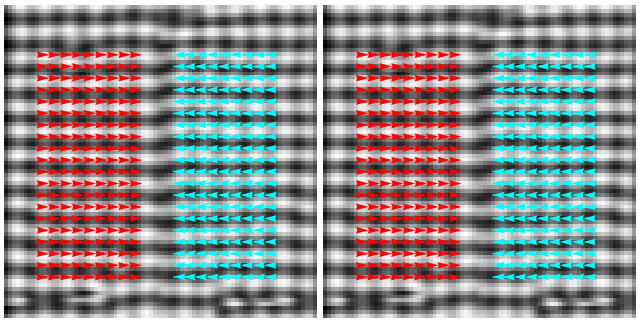

Figure 3: Comparison of vector fields in the artificial sequence. Extracted vector field (left) and ground truth (right).

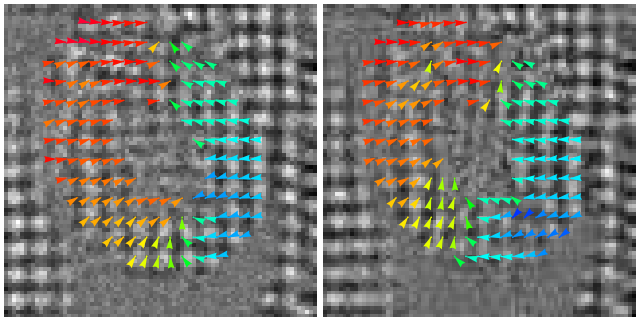

Figure 4: Flow field of MR images sequence, representing a mouse heart in phase of contraction. The sequence consisted of 7 frames and the filtered velocity field of the third and fifth frame has been displayed in the picture. The direction of the velocity vectors is color-encoded, the colors provide information about the coherency of the flow field in certain regions.

brightness methods are sensitive to the tag fading; the MR images have to be filtered in the Fourier domain in order to extract the velocity field. In this process the tag fading and noise are eliminated, but also information about the movement of the tags. Feature based optic flow methods are not dependent on constant brightness and less sensitive to tag fading, which makes our approach suitable for clinical practice. Future tests will include the evaluation of our method directly on MR images. In the experiments the velocity field of our approach has been extracted at fixed scales. In real data, due to deformation of the cardiac walls, the structure changes scale over time, thus, the final results obtained in the assessment may not be optimal. Therefore, it may be interesting to repeat the same experiments by using a scale selection method. Finally, the behavior of the cardiac muscle is characterized by twistings and contractions, therefore, interpolation with a term, that takes into account the rotation and the expansion of the vector field may improve the results.

References

[1] H.C. Van Assen, L.M.J. Florack, A. Suinesiaputra, J.J.M. Westenberg, and B.M. ter Haar Romeny. Purely evidence based multiscale cardiac tracking using optic flow. In *MICCAI 2007 workshop on Computational Biomechanics for Medicine II*, pages 84 – 93. Springer-Verlag, 2007. 1

[2] L. Axel and L. Dougherty. Mr imaging of motion with spatial modulation of magnetization. *Radiology*, 171(3):841–845, 1989. 2

[3] J.L. Barron, D.J. Fleet, and S. Beauchemin. Performance of optical flow techniques. *International Journal of Computer Vision (IJCV1994)*, 12(1):43–77, 1994. 2.5

[4] J. Blom. Affine invariant corner detection, 1991. Dissertation for the Dutch PhD degree, Utrecht University, Utrecht, The Netherlands. 2.3

[5] B. Brox, A. Bruhn, N. Papenberg, and J. Weickert. High accuracy optical flow estimation based on a theory for warping. In *Proceedings of the 8th European Conference on Computer Vision*, volume 3024, pages 25–36. SV, 2004. 1

[6] A. Bruhn, J. Weickert, T. Kohlberger, and C. Schnoerr. A mutigrid platform for real-time motion computation with discontinuity-preserving variational methods. *International Journal of Computer Vision*, 70(3):257–277, 2006. 1

[7] S. E. Fischer, G.C. McKinnon, S.E. Maier, and P. Boesiger. Improved myocardial tagging contrast. *Magnetic Resonance in Medicine*, 30(2):191–200, 1993. 2

[8] L. Florack. *Image Structure*, volume 75 of *Computational Imaging and Vision*. Kluwer Academic Publishers, Utrecht, The Netherlands, first edition, 1997. 1, 2.1

[9] L. Florack, W. Niessen, and M. Nielsen. The intrinsic structure of optic flow incorporating measurement duality. *International Journal of Computer Vision*, 27(3):263–286, 1998. 1

[10] L. M. J. Florack, B. M. ter Haar Romeny, and M. A. Viergever. Scale and the differential structure of images. *Image and Vision Computing*, 10(6):376–388, 1992. 2.3

[11] L.M.J. Florack and H.C. Van Assen. Dense multiscale motion extraction from cardiac cine mr tagging using harp technology. In *Proc. Mathematical Methods in Biomedical Image Analysis. Workshop of the ICCV*, 2007. 1

[12] B.K.P Horn and B.G. Shunck. Determining optical flow. *Artificial Intelligence*, 17:185–203, 1981. 1

[13] J.J. Koenderink. The structure of images. *Biol. Cybern*, 50:363–370, 1984. 2.1

[14] T. Lindeberg. *Scale-Space Theory in Computer Vision*. The Springer Intern. Series in Engineering and Computer Science. Kluwer Academic Publishers, Dodrecht, The Netherlands, first edition, 1994. 2.1

[15] B. Lucas and T. Kanade. An iterative image registration technique with application to stereo vision. In *Proc. DARPA, Image Process*, volume 21, pages 85–117, 1981. 1

[16] W.J. Niessen, J.S. Duncan, L.M.J. Florack M. Nielsen, B.M. ter Haar Romeny, and M.A. Viergever. A multiscale approach to image sequence analysis. *Computer Vision and Image Understanding*, 65(2):259–268, 1997. 1

[17] W.J. Niessen, J.S. Duncan, B.M. ter Haar Romeny, and M.A. Viergever. Spatiotemporal analysis of left ventricular motion. In *Medical Imaging 95,San Diego,SPIE*, pages 192–203, 1995. 1

[18] N.F. Osman, W.S. McVeigh, and J.L. Prince. Cardiac motion tracking using cine harmonic phase (harp) magnetic resonance imaging. *Magnetic Resonance in Medicine*, 42(6):1048–1060, 1999. 2

[19] W Rosamond, K Flegal, K Furie, A Go, K Greenlund, N Haase, S M Hailpern, M Ho, V Howard, B Kissela, S Kittner, D Lloyd-Jones, M McDermott, J Meigs, C Moy, G Nichol, C O'Donnell, V Roger, P Sorlie, J Steinberger, T Thom, M Wilson, and Hong, Y; American Heart Association Statistics Committee and Stroke Statistics Subcommittee. Heart Disease and Stroke Statistics 2008 Update. A Report

From the American Heart Association Statistics Committee and Stroke Statistics Subcommittee. *Circulation*, 117:e2–e122, 2008. 1

[20] S. Sampath, J.A. Derbyshire, E. Atalar, N.F. Osman, and J.L. Prince. Realtime imaging of twodimensional cardiac strain using a harmonic phase magnetic resonance imaging (harpmri) pulse sequence. *Magnetic Resonance in Medicine*, 50(1):154–163, 2003. 2

[21] J. Staal, S. Kalitzin, B. M. ter Haar Romeny, and M. Viergever. Detection of critical structures in scale space. In *Lecture Notes In Computer Science*, volume 1682 archive Proceedings of the Second International Conference on Scale-Space Theories in Computer Vision, pages 105–116, 1999. 2.2

[22] A. Suinesiaputra, L.M.J. Florack, J.J.M. Westenberg, B.M. ter Haar Romeny, J.H.C. Reiber, and B.P.F. Lelieveldt. Optic flow computation from cardiac mr tagging using a multiscale differential method a comparative study with velocity encoded mri. In *Proceedings of the Sixth International Conference on Medical Image Computing and Computer-Assisted Intervention MICCAI 2003*, pages 483–490. LNCS, Berlin, Springer-Verlag, November 2003. 1

[23] B. M. ter Haar Romeny. *Front-End Vision and Multi-Scale Image Analysis: Multiscale Computer Vision Theory and Applications, written in Mathematica*. Computational Imaging and Vision. Kluwer Academic Publishers, Eindhoven, The Netherlands, first edition, 2003. 2.1, 2.2, 2.3

[24] E.A. Zerhouni, D.M. Parish, W.J. Rogers, A. Yang, and E.P. Sapiro. Human heart: tagging with mr imaginga method for noninvasive assessment of myocardial motion. *Radiology*, 169(1):59–63, 1988. 2